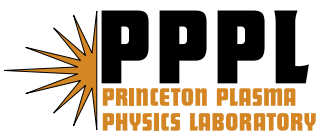# Princeton Plasma Physics Laboratory

Experimental Simulations of Beam Propagation over Large Distances in a Compact Linear Paul Trap

Erik P. Gilson, Moses Chung, Ronald C. Davidson
Mikhail Dorf, Philip C. Efthimion, and Richard Majeski

October 2006

PPPL
PRINCETON PLASMA
PHYSICS LABORATORY

Princeton Plasma Physics Laboratory
Report Disclaimers

PPPL Report Availability

Princeton Plasma Physics Laboratory:

http://www.pppl.gov/pub_report/

Office of Scientific and Technical Information (OSTI):

http://www.osti.gov/bridge

U.S. Department of Energy:

U.S. Department of Energy
Office of Scientific and Technical Information
P.O. Box 62
Oak Ridge, TN 37831-0062
Telephone: (865) 576-8401
Fax: (865) 576-5728
E-mail: reports@adonis.osti.gov

Experimental simulations of beam propagation over large distances in a compact linear Paul trap[a)]

Erik P. Gilson,[b)] Moses Chung, Ronald C. Davidson, Mikhail Dorf,
Philip C. Efthimion, and Richard Majeski
Plasma Physics Laboratory, Princeton University, Princeton, New Jersey 08543

The Paul Trap Simulator Experiment (PTSX) is a compact laboratory experiment that places the physicist in the frame of reference of a long, charged-particle bunch coasting through a kilometers-long magnetic alternating-gradient (AG) transport system. The transverse dynamics of particles in both systems are described by similar equations, including nonlinear space-charge effects. The time-dependent voltages applied to the PTSX quadrupole electrodes are equivalent to the axially oscillating magnetic fields applied in the AG system. Experiments concerning the quiescent propagation of intense beams over large distances can then be performed in a compact and flexible facility. An understanding and characterization of the conditions required for quiescent beam transport, minimum halo particle generation, and precise beam compression and manipulation techniques, are essential, as accelerators and transport systems demand that ever-increasing amounts of space charge be transported. Application areas include ion-beam-driven high energy density physics, high energy and nuclear physics accelerator systems, etc. One-component cesium plasmas have been trapped in PTSX that correspond to normalized beam intensities, $\hat{s} = \omega_p^2(0)/2\omega_q^2$, up to 80% of the space-charge limit where self-electric forces balance the applied focusing force. Here, $\omega_p(0) = [n_b(0)e_b^2/m_b\epsilon_0]^{1/2}$ is the on-axis plasma frequency, and ω_q is the smooth-focusing frequency associated with the applied focusing field. Plasmas in PTSX with values of $\hat{s}$ that are 20% of the limit have been trapped for times corresponding to equivalent beam propagation over 10 km. Results are presented for experiments in which the amplitude of the quadrupole focusing lattice is modified as a function of time. It is found that instantaneous changes in lattice amplitude can be detrimental to transverse confinement of the charge bunch. © *2006 American Institute of Physics.*
[DOI: 10.1063/1.2192760]

I. INTRODUCTION

Intense beam propagation[1–6] is an active area of research and is at the center of various scientific studies, including heavy ion fusion, spallation neutron sources, high energy physics, nonlinear dynamics, and nuclear waste transmutation.[7] The Paul Trap Simulator Experiment (PTSX) simulates, in a compact cylindrical Paul trap,[8] intense beams with normalized intensity parameter $\hat{s}$ up to 0.8[9] (as defined in the following) that propagate for equivalent distances of over 10 km.[9] This allows the study of important scientific topics such as: the conditions for quiescent beam propagation, collective mode excitation, beam-mismatch effects, generation and dynamics of halo particles, and distribution function effects.[10–13] At the high beam intensities envisioned in present and next-generation facilities, a fundamental understanding of the influence of collective processes and self-field effects on beam transport and stability properties must be developed.

In intense charged particle beams, the space-charge effects are sufficiently strong that they affect the dynamics of the beam propagation. The strength of the transverse space-charge force is characterized by the plasma frequency $\omega_p(r) = [n_b e_b^2/m_b\epsilon_0]^{1/2}$, whereas the transverse confining force is characterized by the average smooth-focusing frequency ω_q of the transverse oscillations of a particle in an alternating-gradient (AG) system.[1] Here, ϵ_0 is the permittivity of free space, $n_b(r)$ is the radial density profile, and e_b and m_b are the ion charge and mass, respectively. The normalized intensity parameter $\hat{s} = \omega_p^2(0)/2\omega_q^2$ describes whether the beam is emittance dominated ($\hat{s} \ll 1$) or space-charge dominated ($\hat{s} \rightarrow 1$). For example, Fermilab's Tevatron injector typically operates at $\hat{s} \sim 0.15$, and the Spallation Neutron Source is expected to operate at $\hat{s} \sim 0.2$. The PTSX device presently operates in the range $0 \leq \hat{s} \leq 0.8$.[9]

Using a linear Paul trap confining a one-component plasma to study beam dynamics was proposed by Davidson *et al.*[14] and by Okamoto and Tanaka.[15] The $e_b\mathbf{E}_\perp^{ext}$ forces that the PTSX electrodes exert on the trapped plasma particles are analogous to the $e_b\mathbf{v_z} \times \mathbf{B}_\perp^{ext}$ forces that the AG system exert on the beam particles in the beam frame provided that long, coasting beams that are thin relative to the AG system magnet spacing are considered. Specifically, the amplitude and frequency of the voltage wave form applied to the PTSX electrodes correspond to the quadrupole magnet strength and lattice spacing in the AG system. In addition to the equivalence of the applied forces, the self-field forces in both systems can be described by scalar potentials that obey Pois-
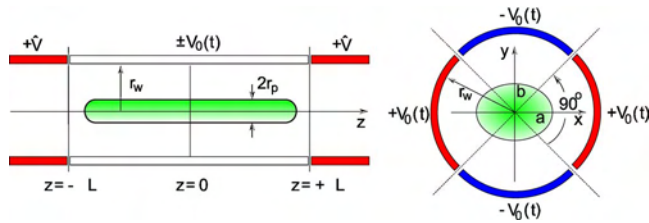
FIG. 1. The PTSX device consists of three cylindrical electrodes with radius $r_w=0.1$ m, each divided into four 90° sectors. An oscillating voltage $\pm V_0(t)$ confines the plasma in the transverse plane to a radius r_p. Static voltages $+\hat{V}$ on the end electrodes confine the ions axially within a length $2L=2$ m.

son's equation. In Ref. 14, it was shown that the self-consistent transverse Hamiltonians and the resulting Vlasov equations for the AG system and the PTSX system are equivalent, neglecting end effects. Thus, the very good confinement properties of ions in PTSX and the arbitrary form of the voltage wave form applied to the confining electrodes make PTSX a compact, flexible laboratory facility in which to simulate intense beam propagation through AG systems.

In this article, a description of the PTSX device is given (Sec. II), related theoretical analyses are summarized (Sec. III), and experimental results that examine the effects of varying both the amplitude and frequency of the applied voltage wave form are presented (Sec. IV). These results are consistent with a smooth-focusing global radial force-balance model for PTSX parameters in the regime where the model is applicable.

II. EXPERIMENTAL APPARATUS

The PTSX device has been described elsewhere[16–18] and only a brief description is presented here. The PTSX device (see Fig. 1) is a linear Paul trap and consists of three colinear cylinders with radius $r_w=0.1$ m, each divided into four 90° azimuthal sectors, in a vacuum of 5×10^{-9} Torr. The pure-cesium-ion plasma is confined radially in the central 2 m long cylinder by oscillating voltages (less than 400 V and less than 100 kHz) applied as shown in Fig. 1. The outer two cylinders are each 0.4 m long and the voltage on these electrodes is held fixed at 150 V in order to confine the plasma axially. To inject or dump the ions, the voltage on one or the other set of outer electrodes is switched to the same oscillating voltage that is applied to the central cylinder. The time duration of injection (t_i), trapping (t_t), and dumping (t_d) may be varied independently with typical values being $t_i=5$ ms, $t_t \le 300$ ms, and $t_d \ge 10$ ms.

The cesium ion source consists of an aluminosilicate emitter surrounded by a Pierce electrode, followed by an acceleration grid and a deceleration grid to extract the desired ion current and adjust the final ion kinetic energy. Extraction voltages of less than 10 V are required to extract sufficient cesium current to fill the trap to a normalized intensity parameter of $\hat{s}=0.8$. Values of the normalized intensity parameter closer to unity have not been achieved in PTSX because the ion source is not ideal and, further, the source injects plasmas that are not perfectly matched to the time-dependent oscillating voltage wave form. These effects cause the trapped plasma to have a large enough effective

transverse temperature that a significant portion of the confining force must be utilized to counteract the thermal pressure when it could otherwise be used to balance the space-charge of a denser plasma.

At the opposite end of PTSX from the ion source, there is a 5 mm diameter circular copper collector. The collector is moveable in the transverse direction in order to measure the z-integrated radial charge profile. This collector moves along a null of the time-dependent applied voltage wave form in order to minimally disturb the electrostatic potential structure. Due to the relatively low axial velocity of ions in PTSX, it takes several milliseconds, or several hundred lattice periods, for the trapped plasma to be completely collected. The measured charge profile is therefore necessarily time averaged.

III. THEORETICAL CONCEPTS

The details of the analogy between AG systems and linear Paul traps such as PTSX are presented in Ref. 14. Here, we discuss the smooth-focusing transverse oscillation frequency ω_q, the smooth-focusing vacuum phase advance σ_v^{sf}, and the force-balance equation that determines the root mean square (rms) beam radius. The transverse motion of particles in either an AG system or in a Paul trap consists of rapid micromotion arising from the periodic focusing and defocusing forces, plus a guiding-center oscillation. In the smooth-focusing approximation, for sufficiently small vacuum phase advance σ_v^{sf}, the time scales of the two motions are well separated. The oscillation frequency of the average transverse motion ω_q, neglecting space-charge effects, is then given by a simple analytical formula.[1,9] The change in phase of this transverse motion over one oscillation period of the focusing system is the smooth-focusing vacuum phase advance σ_v^{sf}.

In the PTSX system, transverse confinement can be described in terms of a ponderomotive force acting on the particles. For the circular PTSX electrodes, the applied electric potential near the axis at $r=0$ is[14]

$$e_b \phi_{\text{ap}}(x,y,t) = \frac{1}{2} \kappa_q(t)(x^2 - y^2), \qquad (1)$$

where $\kappa_q(t)=8e_b V_0(t)/m_b \pi r_w^2$. The voltage applied to the electrodes has the form $\pm V_0(t)=\pm V_{0\,\text{max}} g(t)$, and $g(t)$ is a periodic function with unit amplitude and frequency f. For $r/r_w \ll 1$, the resulting ponderomotive force is proportional to the displacement from the axis, and the frequency of the transverse oscillations is given in the smooth-focusing approximation by[1,9,16,17]

$$\omega_q = \frac{8e_b V_{0\,\text{max}}}{m_b r_w^2 \pi f} \xi, \qquad (2)$$

where $m_b=133$ amu for Cs$^+$ ions in PTSX. The factor ξ depends on the shape of the voltage wave form $g(t)$: $\xi=(1/2)\sqrt{2\pi}$ for a sinusoidal wave form, and $\xi=4\sqrt{3}/(\eta\sqrt{3-2\eta})$ for a periodic step-function wave form with fill-factor η (the so-called focusing-off-defocusing-off, or FODO lattice). Further, the smooth-focusing vacuum phase advance σ_v^{sf} is given by $\sigma_v^{\text{sf}}=\omega_q/f$.[1,9,16,17]

Under quasi-steady-state conditions, for a thermal equilibrium distribution of particles, the average density profile $n_b(r)$ is given by[1,2]

$$n_b(r) = n_b(r = 0)\exp\left[-\frac{m_b\omega_q^2 r^2 + 2e_b\phi^s(r)}{2kT}\right]. \quad (3)$$

Here, k is Boltzmann's constant, T=const. is the transverse temperature, and the space-charge potential $\phi^s(r)$ is determined self-consistently from Poisson's equation $r^{-1}\partial_r(r\partial_r\phi^s) = -n_b(r)e_b/\epsilon_0$. For $kT \to 0$, the numerator in the exponential must also approach zero in order for the density to remain finite, and this implies a nearly uniform density plasma. In the case of low space-charge density, the electrostatic potential term in the exponential can be neglected and the radial density profile is nearly Gaussian.

Integration of Eq. (3) over the radial distribution gives the global radial force balance equation[1]

$$m_b\omega_q^2 R_b^2 = 2kT + \frac{N_b e_b^2}{4\pi\varepsilon_0}, \quad (4)$$

where $N_b = \int_0^{r_w} n_b(r)2\pi r\, dr$ is the line density, and $R_b^2 = (1/N_b)\int_0^{r_w} n_b(r)2\pi r^3\, dr$ is the mean-square radius of the plasma column. As alluded to previously when discussing the observed limit of $\hat{s} = 0.8$ in PTSX, Eq. (4) states that the applied confining force must balance both the thermal pressure and the repulsive space-charge force. In PTSX experiments, R_b^2 and N_b are calculated from the measured plasma density profiles; kT is the only parameter not known *a priori* and is inferred from Eq. (4).

IV. EXPERIMENTAL RESULTS

For the first data presented here, the voltage applied to the 0.6 in. diameter emitting surface of the cesium source was 3 V, whereas the voltage on the acceleration grid was varied between 2.5 and 0 V. The deceleration grid was held fixed at 0 V. The electrodes were driven with sinusoidal wave forms with a 235 V amplitude and a 75 kHz frequency so that $\omega_q = 6.51 \times 10^4$ s^{-1} and $\sigma_v^{sf} = 49.7°$. The plasmas were injected for 5 ms, trapped for 1 ms, and then dumped. The radial charge profile, which is proportional to $n_b(r)$, is then measured by averaging the signal at each radial position over several hundred shots of PTSX. The area of the collector aperture and an estimate of the plasma length L_p (Ref. 19) are then used to calculate $n_b(r)$. Typical peak densities are less than 5×10^5 cm^{-3}. Given temperatures of approximately 0.5 eV,[9] the Debye length is 0.8 cm, which makes these moderate-intensity plasmas several Debye lengths in transverse extent.

To make use of Eq. (4) in order to measure the effective transverse temperature of the plasma, N_b and R_b are obtained from the experimental data by integrating the appropriate moments of the measured radial density profile $n_b(r)$ of the trapped plasma. The validity of Eq. (4) for PTSX was established in Ref. 9 in which the linear relationship between $m_b\omega_q^2 R_b^2$ and $N_b e_b^2/4\pi\epsilon_0$ was observed. The parameter $\hat{s} = \omega_p^2(0)/2\omega_q^2$ is extracted from the measured density profile $n_b(r)$ by using the on-axis value $n_b(0)$.
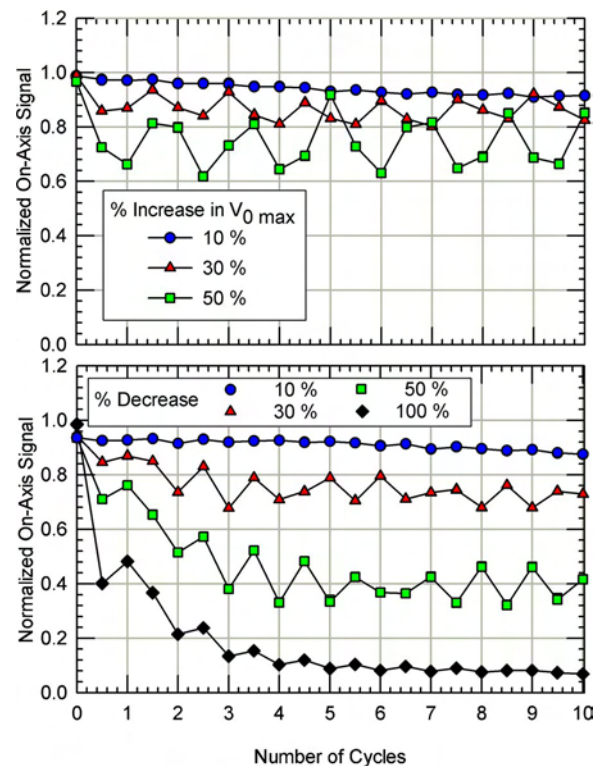

FIG. 2. Instantaneous changes in the voltage wave form amplitude cause envelope oscillations that result in various amounts of transverse heating, and thus various amounts of radial expansion and corresponding central density decrease.

The first set of experiments presented here corresponds to the case of a malfunctioning quadrupole magnet set in the AG system and is simulated by changing the amplitude of the voltage wave form from its initial value $V_{0\,max} = V_1$ to a voltage $V_{0\,max} = V_2$ for half-period of the oscillation. In order to measure the resulting envelope oscillation that occurs because the plasma is suddenly mismatched to the transport lattice, the modified voltage V_2 is allowed to persist for a variable number (up to 20) of half-periods before returning to the original value V_1. By performing the experiment in this way, it allows the effect of abrupt changes in the lattice strength to be more fully explored.

Voltage increases of 10%, 30%, and 50% are considered, as are decreases of 10%, 30%, 50%, and even 100% (see Fig. 2). To determine the essence of the effect and to complete the experiment in a timely manner, only $n_b(0)$ is measured rather than the entire radial density profile. As evident from Fig. 2, for voltage increases, the on-axis signal oscillates as a function of the number of cycles for which the voltage V_2 was applied before switching back to V_1. In addition, similar oscillations are evident for the voltage decreases, although there appears to be a beat-wave phenomenon occurring in this case. The decay time in the 100% decrease data corresponds to the transit time for a thermal ion to reach the wall of the system.

The mechanism for this effect can be described qualitatively as follows. After being trapped initially, the plasma rapidly relaxes to a state where the plasma radius is determined by a balance between the applied focusing fields and
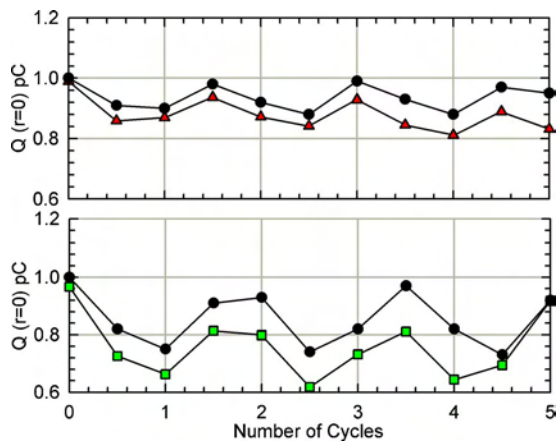
FIG. 3. WARP 2D simulations using the full time-dependent quadrupole field (circles) compare favorably with the experimental data for the 30% increase (triangles) and the 50% increase (squares) in voltage wave form amplitude.

FIG. 4. For the baseline case, $V_{0\,max}=150$ V, $f=60$ kHz, $\omega_q=5.2\times10^4$ s^{-1}, and $\sigma_v^{sf}=50°$. All of the selected points, A through H, have either $f=40$, 60, or 90 kHz. All of the selected points have one parameter $(V_{0\,max}, f, \omega_q, \sigma_v^{sf})$ in common with the baseline case. Some selected points are connected by curves of constant ω_q or constant σ_v^{sf}.

the defocusing effects of the plasma space-charge and thermal pressure. When the applied voltage amplitude abruptly changes to V_2, the new "equilibrium" radius is different, and the plasma envelope begins to oscillate about this new radius. When the voltage amplitude is switched back to its original value V_1, the plasma's radius is different than the original equilibrium radius unless the period of the envelope oscillations is commensurate with the duration of the voltage amplitude change. Therefore, the plasma envelope again oscillates, but now it oscillates about the original equilibrium radius. The amplitude of this final oscillation depends on the phase of the first oscillation at the instant the voltage amplitude returns from V_2 to V_1. Large-amplitude final oscillations lead to large emittance growth and thus larger final plasma radius. Since particle number is conserved, a larger plasma radius implies a smaller on-axis density $n_b(0)$. Small-amplitude final oscillations lead to only modest emittance growth and plasmas whose radius and central density are nearly the same as before the voltage amplitude was changed.

Simulations using the WARP 2D code[20] that employ a smooth-focusing model demonstrate the essence of the effect, but the periodicity of the central-density oscillations with number of cycles does not agree with the experimental data. However, when using the actual oscillating quadrupole fields in the WARP 2D simulations, the agreement between the simulations and the experimental data are excellent, as shown in Fig. 3. Note that the full oscillating quadrupole fields are required in the simulation even though the smooth-focusing vacuum phase advance only increases from 50° to 75°.

In the second set of experiments presented here, instantaneous changes of the voltage wave form amplitude and/or frequency that are sustained until the end of the experiment are considered. An experiment of this sort is relevant because, for example, it might be desirable to compress a beam in as short a propagation distance as possible by modifying the lattice parameters. Although intuition suggests that ins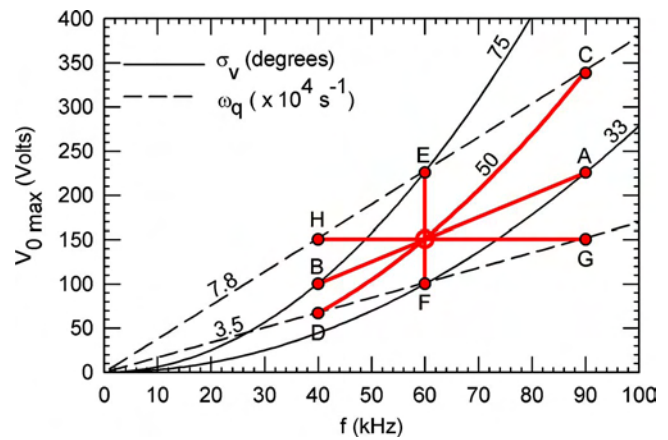tantaneous changes will lead to emittance growth, instantaneous changes are one limiting case of rate-of-change experiments.

Figure 4 shows the PTSX parameter space, the settings for the baseline case, and also the settings for various final voltage and frequency settings after an instantaneous change. These various final settings are related to the baseline case in certain specific ways.

Points A and B have the same transverse focusing frequency ω_q as the baseline case. For case A, both the voltage wave form amplitude and frequency are increased by a factor of 1.5. For case B, both the voltage wave form amplitude and frequency are decreased by a factor of 1.5. The transverse focusing frequency remains fixed since ω_q scales like $V_{0\,max}/f$ [Eq. (2)]. The phase advance must then be different for the baseline case, case A, and case B. Indeed σ_v^{sf} is 33° for case A, 50° for the baseline case, and 75° for case B.

Cases C and D are complimentary to cases A and B in the sense that, for cases C and D, the phase advance is the same as for the baseline case, whereas ω_q is allowed to vary. When the phase advance is held fixed, ω_q then scales like f. The voltages and frequencies for cases C and D were selected so that ω_q is either increased or decreased by a factor of 1.5.

Since one may think of the system parameters either in terms of transverse focusing frequency and phase advance $(\omega_q, \sigma_v^{sf})$, or lattice strength and spacing $(V_{0\,max}, f)$, the instantaneous changes labeled as cases E, F, G, and H are also considered. Cases E and F correspond to a voltage wave form amplitude increase and decrease, respectively, whereas cases G and H correspond to voltage wave form frequency increases and decreases, respectively. The change in voltage or frequency is chosen so that ω_q either increases or decreases by a factor of 1.5.

Having chosen the voltages and frequencies in this way, there are several relationships between the cases that should be pointed out. The baseline case and cases A and B share a common value of ω_q by design. Further, however, cases C, E, and H all correspond to a value of ω_q that is 1.5 times that of the baseline case. Similarly, cases D, F, and G all corre-
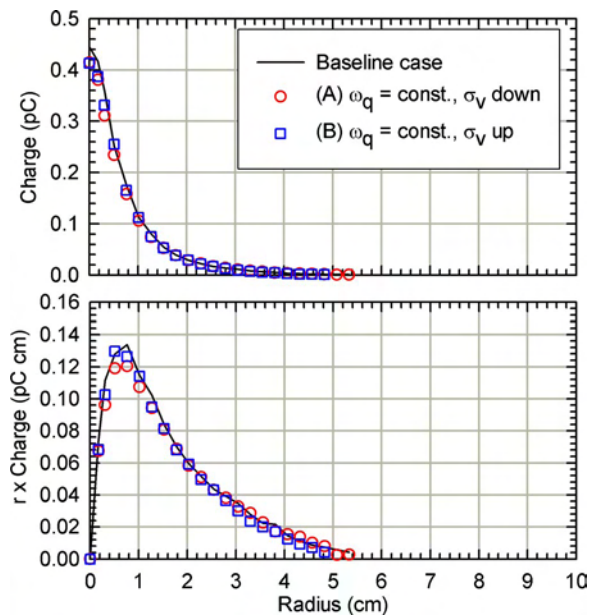
FIG. 5. The measured radial charge profile can be converted into to the radial density profile by dividing by $a_c L_p$ where a_c is the area of the collector and L_p is the length of the plasma column. For simultaneous proportional instantaneous changes in the voltage wave form amplitude and frequency, there is no change in the transverse density profile of the plasma.

FIG. 6. The final-state radial charge profile (and, hence, density profile) is independent of whether $V_{0\,max}$, f, or σ_v^{sf} is kept fixed when ω_q is reduced by a factor of 1.5.

spond to a value of ω_q that is 1.5 times small than that of the baseline case. The baseline case and cases C and D have the same σ_v^{sf} by design. In addition, cases A and F have the same value of σ_v^{sf} as each other, as do cases B and E. This allows for a better experimental check on the dependencies of the effects of instantaneous changes on the lattice parameters.

The baseline case uses a voltage wave form with an amplitude of 150 V and a frequency of 60 kHz, which implies a transverse focusing frequency of 6.5×10^4 s^{-1} and a phase advance of 50°. In these experiments, plasma is trapped for 1 ms before being dumped for diagnosis. Specifically, for the baseline case, the plasma is trapped for 60 lattice periods. The baseline case is a plasma with a transverse temperature of 0.7 eV and a normalized intensity parameter $\hat{s}=0.2$. The instantaneous transitions are implemented half way through the trapping period. Thus, after being held for 30 lattice periods before applying the instantaneous change, the plasma is held for: another 20 lattice periods for cases B, D, and H; another 30 lattice periods for cases E and F; and another 45 lattice periods for cases A, C, and G. Recall that it takes several milliseconds, or hundreds of lattice periods, for the plasma to be collected by the diagnostic.

Figure 5 shows the results for cases A and B in which the transverse focusing frequency is held fixed by increasing or decreasing $V_{0\,max}$ and f in equal proportion. There is not a discernible change in the radial density profile despite the fact that the wave form voltage amplitude and frequency are each changed by factor of 1.5. Even for case A, where the vacuum phase advance is 75°, the phase advance is still small enough that the exact phase advance differs from the smooth-focusing phase advance by only 13%. One then expects that the smooth-focusing model is sufficient to describe
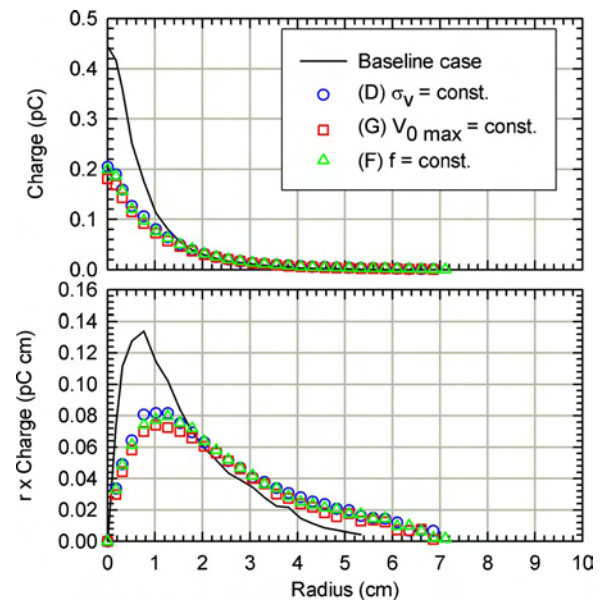
the data. Indeed, in the smooth-focusing approximation, the rapid oscillations at the lattice frequency do not appear, and the state of the plasma is independent of the phase advance.

The key role of ω_q is confirmed by examination of the data in Fig. 6, where the results for cases D, F, and G are shown. These are the cases in which ω_q has been lowered by a factor of 1.5, while either keeping $V_{0\,max}$, f, or σ_v^{sf} fixed. Even though the final voltage wave form amplitudes and frequencies vary over a wide range in these three cases, the radial density profiles are nearly indistinguishable from one another. The largest phase advance is for case D and is only 50°, and the results can be understood in the context of the smooth focusing model. The force-balance equation (4) states that a lower ω_q will lead to a larger beam radius R_b if the line charge N_b and the temperature kT are fixed. The emittance, which scales like $\epsilon \propto R_b \sqrt{kT}$, increases by 45% in Fig. 6. Note, however, that the normalized intensity remains $\hat{s}=0.2$.

The study is completed by considering the results of cases C, E, and H, shown in Fig. 7. In these cases, the final ω_q is 1.5 times larger than in the baseline case. However, these instantaneous changes now lead to three distinct radial density profiles despite having the same final ω_q.

The parameter change in case E, an instantaneous change to a larger voltage wave form amplitude, and a vacuum phase advance of 75°, results in a larger on-axis plasma density and a warmer plasma. This is qualitatively what is expected; an increase in ω_q gives a smaller R_b [and thus larger $(n_b(0)]$ when N_b is fixed, provided the increase in kT is not too large. If the increase in kT is sufficiently large, then as ω_q increases, R_b may increase as well. Nevertheless, it is observed for case E in Fig. 7 that the increase in on-axis plasma density is offset by the increase in ω_q so that the normalized intensity drops to $\hat{s}=0.14$. Further, the emittance has increased by 40%.
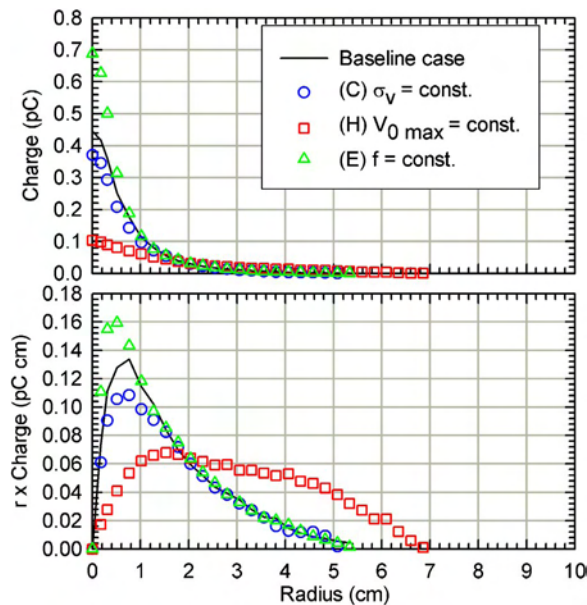
FIG. 7. When ω_q increases and the effective temperature T increases as well, then R_b may either increase or decrease as necessary in order to maintain radial force balance. A sudden transition to a large value of σ_v^{sf} leads to a drastic change in the shape and temperature of the plasma.

The parameter change in case C in Fig. 7, an instantaneous change to a larger voltage wave form amplitude and frequency at a constant phase advance of 50°, results in a smaller on-axis plasma density and a higher effective transverse temperature than the baseline case. The temperature increase is greater than that in case E, and in fact is large enough to cause sufficient radial broadening of the plasma so that the on-axis density decreases. The emittance has increased by 60%. A possible source for the larger transverse heating is the larger envelope oscillation induced by the sudden change of system parameters to a point in the high-voltage/high-frequency region of parameter space. When the frequency is large, the PTSX electrode impedance becomes small and, therefore, a high-voltage/high-frequency operating point places the greatest burden on the electrode driver circuitry. Specifically, bandwidth and slew rate limits cause the sinusoidal wave form to become distorted.

The parameter change in case H in Fig. 7 is unique as compared to the others in this study in that the vacuum phase advance for the parameters in case H is large; $\sigma_v^{sf} = 112°$. In this regime, the discrepancy between the smooth focusing phase advance and the actual vacuum phase advance is large since the assumptions of the smooth-focusing model are breaking down. The exact vacuum phase advance for case H in Fig. 7 is calculated to be $\sigma_v = 150°$. This is near the instability limit for single-particle orbits, and to detect many particles moving to large radius is therefore not surprising. The emittance change for case H in Fig. 7 is 450%.

V. CONCLUSIONS

The PTSX device is being used to study the dynamics of intense beam propagation over large equivalent distances through magnetic alternating-gradient transport systems, but in a compact laboratory setting. This is possible because the equations that describe the transverse dynamics of particles in the two systems are similar. Measurements of the envelope oscillations that occur after a sudden, but temporary, change in amplitude of the confining field have been performed and are in excellent agreement with computer simulations when the full time-dependent quadrupolar confinement fields are employed in the simulation.

The smooth-focusing global force balance equation is sufficient to interpret experiments in which instantaneous changes in voltage wave form amplitude and/or frequency are made. One notable exception is when the vacuum phase advance becomes too large. When the transverse focusing frequency is reduced, then the plasma radius must increase, and more so if the transverse plasma temperature also increases. When the transverse focusing frequency does not change, it is observed that there is no effect on the plasma, including an absence of noticeable transverse heating. When the transverse focusing frequency increases, whether the plasma radius increases or not depends on the amount of transverse heating that is caused by the suddenly induced mismatch. When the transverse focusing frequency is changed instantaneously, the transverse emittance increases by 40% or more.

[1] R. C. Davidson and H. Qin, *Physics of Intense Charged Particle Beams in High Intensity Accelerators* (World Scientific, Singapore, 2001).

[2] M. Reiser, *Theory and Design of Charged Particle Beams* (Wiley, New York, 1994).

[3] A. W. Chao, *Physics of Collective Beam Instabilities in High Energy Accelerators* (Wiley, New York, 1993).

[4] P. G. O'Shea, M. Reiser, R. A. Kishek, S. Bernal, H. Li, M. Pruessner, V. Yun, Y. Cui, W. Zhang, Y. Zou *et al.*, Nucl. Instrum. Methods Phys. Res. A **464**, 646 (2001).

[5] N. Kjærgaard and M. Drewsen, Phys. Plasmas **8**, 1371 (2001).

[6] See, for example, *Proceedings of the 2003 Particle Accelerator Conference* (IEEE, Piscataway, NJ, 2003), IEEE Catalog Number 01CH37423, pp. 1–3571.

[7] See, for example, Proceedings of the International Heavy Ion Fusion Symposium, Nucl. Instrum. Methods Phys. Res. A 1 (2005).

[8] W. Paul and H. Steinwedel, Z. Naturforsch. A **8**, 448 (1953).

[9] E. P. Gilson, R. C. Davidson, P. C. Efthimion, and R. Majeski, Phys. Rev. Lett. **92**, 155002 (2004).

[10] S. M. Lund and B. Bukh, Annu. Rev. Astron. Astrophys. **7**, 024801 (2004).

[11] L. K. Spentzouris, J.-F. Ostiguy, and P. L. Colestock, Phys. Rev. Lett. **76**, 620 (1996).

[12] D. Neuffer, E. Colton, D. Fitzgerald, T. Hardek, R. Hutson, R. Macek, M. Plum, H. Thiessen, and T.-S. Wang, Nucl. Instrum. Methods Phys. Res. A **321**, 1 (1992).

[13] J. Byrd, A. Chao, S. Heifets, M. Minty, T. O. Raubenheimer, J. Seeman, G. Stupakov, J. Thomson, and F. Zimmerman, Phys. Rev. Lett. **79**, 79 (1997).

[14] R. C. Davidson, H. Qin, and G. Shvets, Phys. Plasmas **7**, 1020 (2000).

[15] H. Okamoto and H. Tanaka, Nucl. Instrum. Methods Phys. Res. A **437**, 178 (1999).

[16] E. P. Gilson, R. C. Davidson, P. C. Efthimion, R. Majeski, and H. Qin, Laser Part. Beams **21**, 549 (2003).

[17] E. P. Gilson, R. C. Davidson, P. C. Efthimion, R. Majeski, and H. Qin, in *Proceedings of the 2003 Particle Accelerator Conference* (IEEE, Piscat-

away, NJ, 2003), IEEE Catalog No. 03CH37423C, p. 2655.

[18] E. P. Gilson, M. Chung, R. C. Davidson, P. C. Efthimion, R. Majeski, and E. A. Startsev, Nucl. Instrum. Methods Phys. Res. A **544**, 171 (2005).

[19] E. P. Gilson, R. C. Davidson, P. C. Efthimion, R. Majeski, and E. A. Startsev, AIP Conf. Proc. **692**, 211 (2003).

[20] A. Friedman, D. P. Grote, and I. Haber, Phys. Fluids B **4**, 2203 (1992).